Magnitude and Frequency of Forces on a Low-Reynolds VAWT Airfoil Using High-Order LES

Samuel Kanner *and Per-Olof Persson†

University of California, Berkeley, Berkeley, CA 94720-3840, U.S.A.

A high-order Implicit Large Eddy Simulations (ILES) method in 2D and 3D is used to simulate a section of a constant spinning straight-bladed vertical-axis wind turbine with two blades at low-Reynolds ($Re \leq 10^5$). The magntiude and frequency content of the blade forces are analyzed and compared to analytical codes and experiments. The maximum power coefficient was found at a tip-speed ratio of 5.0. The pitch angle of the blades was also varied in order to take into account the uncertainties in the mounting angle of the blade in the experimental studies. As found previously, a small toe-out angle can increase the power absorption of the turbine by nearly 10%. Over a range of tip-speed ratios, the computed tangential forces as a function of the azimuthal angle agree much better to the experimental data at high tip-speed ratios as compared to other, lower-fidelity analytical turbine codes. The wake structures are visualized using the q-criterion at various azimuthal angles and tip-speed ratios and the dominant frequencies of the tangential force are reported.

Nomenclature

A_v	Swept area of VAWT	H	Vertical height of VAWT blade
c	Chord length of VAWT blade	N_b	Number of VAWT blades
c_0	Distance from LE along chord line of mount point	R	VAWT radius at equator
C_D	Sectional airfoil drag coefficient, $2F_D/(\rho U_\infty^2 c)$	Re	Chord Reynolds number, $\rho U_\infty c/\mu$
C_L	Sectional airfoil lift coefficient, $2F_L/(\rho U_\infty^2 c)$	t^*	Normalized time, tU/c
C_p	Sectional power coefficient of turbine, $2P/(\rho U_\infty^3 A_v)$	U_∞	Free-stream horizontal fluid velocity
C_T	Sectional VAWT tangential force coefficient, $2F_T/(\rho U_\infty^2 c)$	*Symbols*	
		α	Angle of attack of airfoil
		α_0	Preset pitch angle of airfoil
		λ	Tip-speed ratio of VAWT, $R\omega/U_\infty$
		ω	Angular velocity of VAWT rotor

I. Introduction

Throughout the 1970s and into the 1980s, Sandia National Laboratories conducted research into the design and testing of vertical-axis wind turbines (VAWTs). At that time, the nascent wind energy industry had not converged on a single optimal design, such as the three-bladed upwind horizontal-axis seen widely today. Recently, however, there has been renewed interest in commercializing VAWTs, especially in an offshore setting. Due to their lower center of gravity and more accessible electromechanical components, VAWTs could

*Ph.D. Candidate, Department of Mechanical Engineering, University of California, Berkeley, Berkeley CA 94720. E-mail: kanners@berkeley.edu. AIAA Student Member.

†Associate Professor, Department of Mathematics, University of California, Berkeley, Berkeley CA 94720-3840. E-mail: persson@berkeley.edu. AIAA Senior Member.

be a superior technology over HAWTs on a floating platform. Their use in a floating environment could result in lower capital costs (due to the smaller platform) as well as operational and maintenance costs. Though only a few large-scale prototypes of floating wind turbines exist today (see, for instance Ref. 1), many developed countries have a large untapped offshore wind resource in deep water (usually defined as greater than 50m water depth), such as the U.S., U.K., China, Japan, and many others. However, the design, manufacture, and maintenance of even a large-scale *onshore* VAWT has proven to be difficult due to the lack of available accurate data (numerical or experimental) on the magnitude and frequency content of the instantaneous aerodynamic forces on the blades.[2] Further, nearly all analytical models used to model VAWTs require some experimental data in their analysis.

One challenge to predicting forces on a VAWT blade is the large variation in angle of attack of the airfoil as it circumnavigates the central column. At certain tip-speed ratios, namely $\lambda \geq 5$, the angle of attack does not exceed 12°, as depicted in Fig. 1. Previous researchers[3–5] have found that three-dimensional Large Eddy Simulation[6] (LES) is necessary to accurately predict the lift and drag of a stalled airfoil. At the lowest TSR ($\lambda \leq 1$), Li *et al*[5] showed that 3D LES (this form of LES is sometimes called 2.5D LES) could accurately predict the tangential force of a straight-bladed VAWT at $Re = 10^5$. However at higher TSR ($1.4 \leq \lambda \leq 2$, the 3D LES model could not accurately predict the forces, especially in the downwind section. For all λ studied in Ref. 5, the maximum tangential forces computed by the 3D URANS simulations were nearly a factor of 2 above the experiments. Though 3D large-eddy simulations (LES) will always exhibit higher fidelity than 2D simulations, the computational cost of such a simulation may be prohibitive. For $\lambda \geq 5$, however, it remains to be determined whether a 2D simulation of a VAWT can accurately predict the forces.

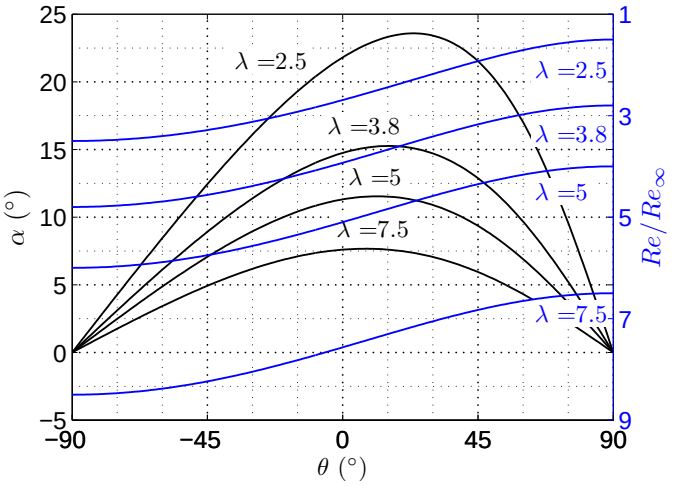

Figure 1. Variation of angle of attack and chord Re of a straight-bladed VAWT as it completes one half rotation.

Although the ILES methodology used in the present study only exhibits adequate stability and robustness properties for $Re < 10^5$, this methodology can still accurately be applied to the unsteady aerodynamics of airfoils with conditions applicable to micro-air vehicles[7] as well as some model-scale VAWTs. For instance, the Reynolds number of the model turbine tested at the Sandia National Labs tow tank is under $50 \cdot 10^3$.[8] The computational efficiency and accuracy of computational fluid dynamics (CFD) simulations have increased dramatically over the past decades. The most common types of simulations, including those found in OpenFOAM, a popular open-source CFD software, are 2D unsteady Reynolds-averaged numerical simulations (URANS). However, these simulations have been found to overestimate the power coefficients of VAWTs due to their delay of the onset of dynamic stall and the overprediction of the tangential force in the upwind zones.[5] In this study, we propose using a high-order ILES method, developed in Ref. 9 for a straight-bladed VAWT. To our knowledge, this is the first study of a high-order ILES code being applied to a VAWT either in 2D or 3D. This methodology can convect the vortices that are created by the VAWT blade in the upwind zone into the downwind zone and accurately simulate the effect of these vortices on a moving blade. Though the present study focuses on VAWTs, these lower-Reynolds results can be used for a variety of new applications, such as unmanned-air vehicles, micro-air vehicles, and the simulation of avian and insect flight.

The paper is organized as follows. First, we describe the ILES method and discretization techniques we used to numerically recreate the 2-bladed VAWT tested by Strickland in Ref. 8. We compare the tangential forces on the VAWT blades in 2D and 3D to the experiments and other anaytical codes. Like Li in Ref. 5, we found that although 2D LES drastically overpredicted the lift and drag coefficients at post-stall angle of attacks, the fidelity of the VAWT simulation did not suffer over a range of TSR. Indeed, we were able to accurately simulate the forces on the VAWT blade in the upwind and downwind zones. Further, we found that the 2D results generally agreed with the 3D results, especially at high tip-speed-ratios. However, the frequency content of the 2D timeseries is generally non-physical, since the vortical structures do not dissipate in the spanwise direction. The frequency content of the 3D simulations, however, can be resolved using classical techniques on a longer timeseries of the tangential force.

II. Methodologies

Our simulations are based on the Navier-Stokes equations, and we use an artificial compressibility method based on an isentropic formulation[10] to approximate the nearly incompressible flows that we are modeling. This results in a system of equations in the conserved variables ρ (density) and $\rho\boldsymbol{u}$ (momentum). We impose two types of boundary conditions, free-stream flow (far field) and zero velocity (wall).

II.A. High-Order Discontinuous-Galerkin Discretization

The equations are discretized using a high-order Discontinuous Galerkin (DG) formulation. While not used routinely for CFD simulations, high order methods have been shown to be advantageous for applications requiring low numerical dispersion and high time accuracy.[11] In particular, they are believed to produce reliable results already on coarse grids for LES simulations with highly separated flows.[9]

We use an in-house developed code for the simulations, which uses high-order DG methods on fully unstructured meshes of tetrahedral elements and nodal basis functions.[12,13] The DG method produces stable discretizations of the convective operator for any order discretization, thus avoiding the need for additional stabilization or filtering. Here, we use polynomial degrees $p = 3$ for all the simulations, which is commonly considered a good compromise between high order accuracy and increased solver cost. The viscous terms are discretized using the Compact Discontinuous Galerkin (CDG) method[14] which leads to optimal order accuracy, is compact, and generates sparser matrices than the alternative existing methods. For the time-integration, we use a 3-stage, 3rd order accurate Diagonally Implicit Runge-Kutta (DIRK) method.

For the turbine simulations, we account for the moving and deforming domains by the mapping based Arbitrary Lagrangian-Eulerian (ALE) formulation proposed in Ref. 12. It is accurate to arbitrary orders in both space and time. The so-called Geometric Conservation Law (GCL) is satisfied using an additional equation that is used to compensate for numerical integration errors. The formulation requires that the deformations are prescribed either explicitly or indirectly as a mapping $x = x(X, t)$ between the reference and the physical space. In our case, we can simply use a rotating framework to model the spinning turbine. We can then analytically compute the deformation gradient $\partial x/\partial X$ and the grid velocity $\partial x/\partial t$, and formulate the ALE equations directly in the reference domain. For details on this procedure, see Ref. 12.

II.B. Model Turbine

The VAWT chosen for this study was the one built and tested by Strickland and reported in Ref. 15 as well as in Ref. 8. Since the model VAWT was actually tested in a tow-tank, the average chord Reynolds number for turbine blades is approximately $40 \cdot 10^3$. A schematic of the experimental test setup is shown in Fig. 2. The width of the tow tank was 5 m, so the effect of the side walls on the turbine blades is negligible. However, the bottom of the blades were only approximately 35 cm away from the bottom of the tank, so the proximity of this boundary on the blades could have a significant effect on the flow around the blades. The physical parameters of the VAWT are shown in Table 1. The definitions of these parameters as well as the definition of the azimuthal angle used for this study are shown in Fig. 3, where the 2-bladed VAWT is shown in plan view. A plot of the variation of the angle of attack as well as the chord Reynolds number for various tip-speed ratios λ is shown in Fig. 1.

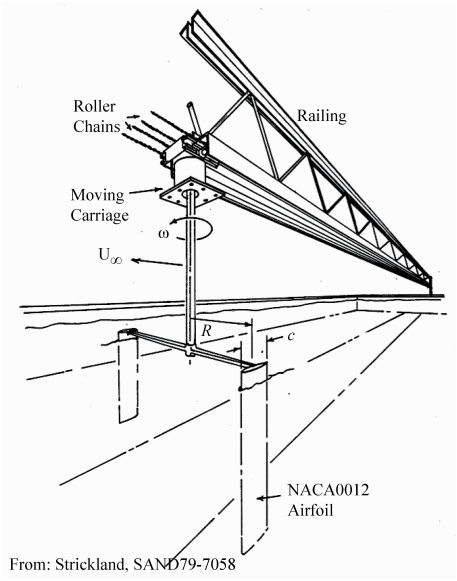

Figure 2. Schematic of tow tank experiment of low Re VAWT performed by Strickland in Ref. 15 and 8.

Parameter	Value	Unit
c	9.14	cm
R	61.0	cm
ω	1.56	rad/s
H	85.0	cm
α_0	-2	deg
c_0	$0.25c$	cm

Table 1. Geometry and turbine parameters for the VAWT simulated in this study.

II.C. Computational Domain

All triangular and tetrahedral meshes are produced using the DistMesh mesh generator.[16] We use a structured approach for the boundary layers around the airfoils, and the 3D meshes are obtained by prismatic extrusion of the triangular elements. In addition, high-order methods require meshes with curved elements, which are particularly difficult to generate for meshes with boundary layers. We use the elasticity-based approach proposed in Ref. 17, which tends to produce well-shaped meshes with globally curved elements.

The computational domain for the VAWT is shown in Fig. 4. We use a very fine mesh in the boundary layer and a finer mesh resolution in the near-wake of the airfoils as compared to the regular domain. The 3D mesh is generated by extruding the 2D mesh, a span of 0.4 chord lengths. The resulting size of the 2D mesh is 11,630 elements, or 116,300 high-order nodes and about 350,000 degrees of freedom. The size of the 3D mesh is 139,560 elements, or about 2.8 million high-order nodes and about 11 million degrees of freedom.

III. Results

In the following section the sectional tangential force coefficient, C_T is displayed as a function of azimuthal angle θ as defined in 3. The sectional tangential force coefficient is usually defined as,

$$C_T = \frac{F_T}{1/2\rho U_\infty^2 c} \tag{1}$$

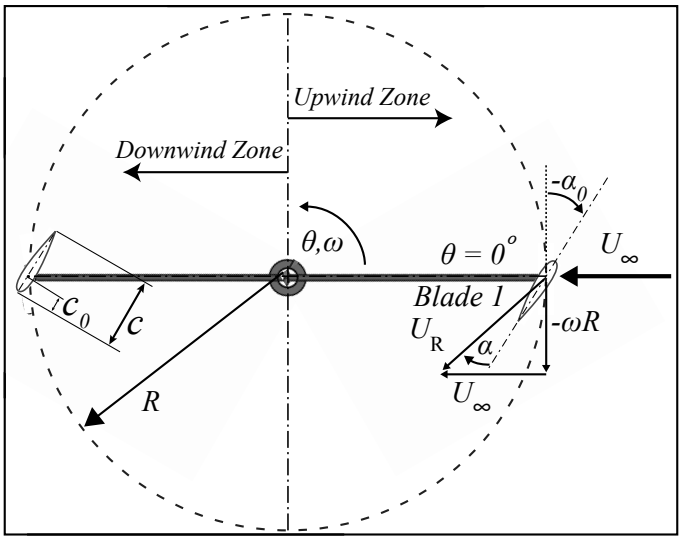

Figure 3. Plan view of 2-bladed VAWT with definitions of angle of attack α, blade offset pitch angle α_0, chord length c, blade offset distance c_0, VAWT radius R, azimuthal angle θ, and VAWT angular velocity ω.

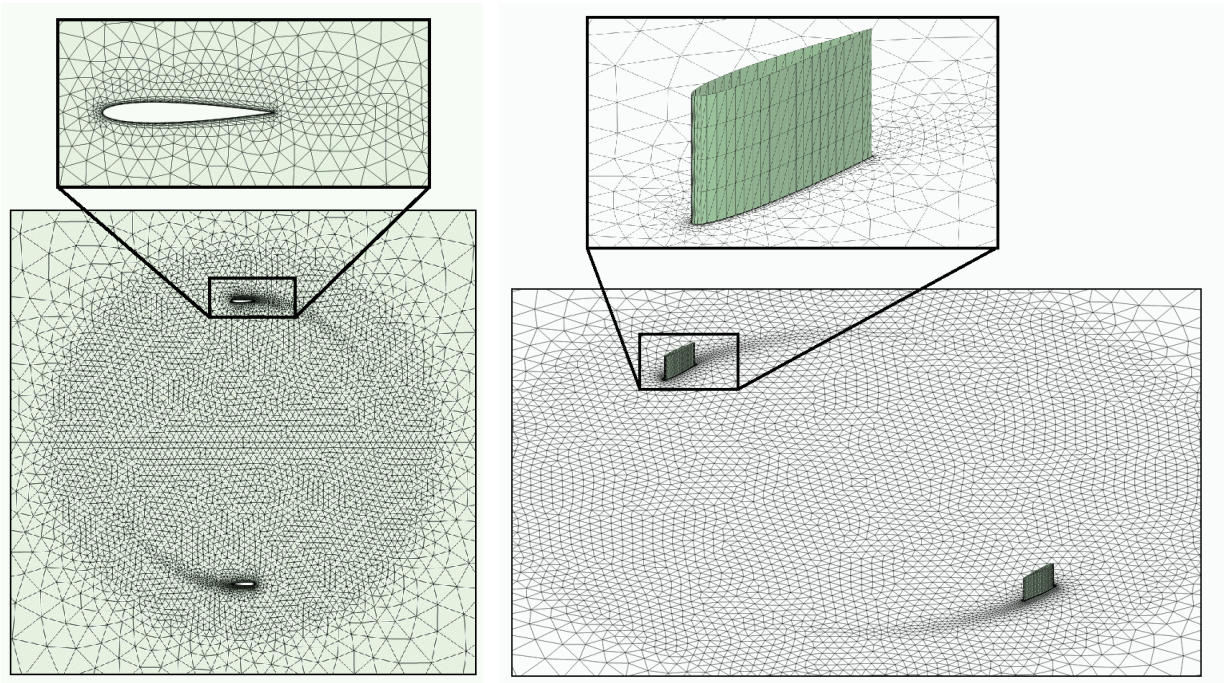

(a) 2D Mesh (b) 3D Mesh

Figure 4. The two high-order computational meshes used for 2D and the 3D simulations of the low Re VAWT considered in this study. Polynomial degrees of $p = 3$ are used within each element.

where F_T is the sectional tangential force on the blade. For a straight-bladed VAWT, the power coefficient C_p is a function of the average of C_T over one revolution, $\bar{C}_T$ and other parameters, such that

$$C_P = N_b \frac{\frac{\omega}{2\pi}\int_0^{2\pi} F_T(\theta) R d\theta}{1/2\rho U_\infty^3 2R} = N_b \frac{\lambda \bar{C}_T}{2}\frac{c}{R} \tag{2}$$

In Ref. 15, the authors do not explicitly report the blade offset distance c_0, which is the distance from the leading edge of the airfoil to the blade mounting point, along the chord line of the airfoil. However, from the discussion on pages 57 and 59 of Ref. 15 on the measurement of the moment about the quarter-chord, we infer that $c_0 = c/4$. From this section, we also infer that the intended blade offset pitch angle α_0 to be 0°. Yet, the authors report uncertainty in the measurement of the azimuthal angle on the order of 1°. The determination of the actual α_0 used in the experiments is discussed in Sec. III.B. In the tow tank experiments, the forces were averaged over a particular time step, which corresponded to a change of $\theta \approx 15°$. In their numerical simulations, they also encountered a phase shift between the numerical results and the experimental results. In the present study, we found that if we shifted θ of the experimental results by -15° only for λ of 2.5 and 7.5 then we found the best agreement with the numerical results from our simulations as well as with the other analytical simulations. All of the following plots include this offset in the azimuthal angle for λ of 2.5, 7.5. Unless otherwise noted, the data from the ILES simulations are the averages over all of the passes of the simulations (usually 2 passes for the 3D simulations and 3-4 passes for the 2D simulations) for Blades 1 and 2 at each of the azimuthal positions.

III.A. Comparison of 2D and 3D ILES

Most of the parameterization study for the ILES simulations were performed in 2D due to the high computational cost of the 3D simulations. In this section, however, we show that the 3D simulations generally follow their 2D counterparts, especially for high TSR. In Fig. 5, the 2D and 3D simulations are compared for $\alpha_0 = -2°$ and $\lambda = 5.0$. The results of the 2D simulations exhibit the same overall behavior as the results from 3D cases, albeit with some higher frequency harmonics. In Fig. 6, the results from the 2D and 3D

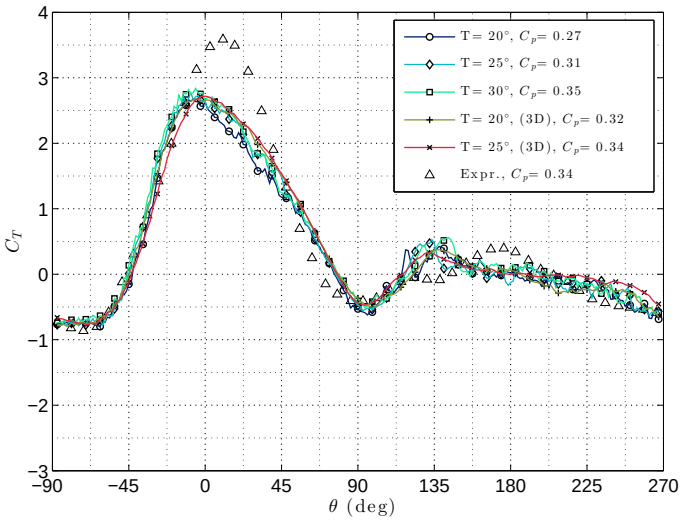

Figure 5. Tangential force of a VAWT blade as a function of azimuthal position for simulations in 2D and 3D $\alpha_0 = -2°$ at $\lambda = 5.0$ for various temperatures.

simulations for $\lambda = 2.5$, $T = 25°$ are shown for different α_0. Here, there are discrepancies between the 2D and 3D simulations, especially for $0° \leq \theta \leq 45°$ Thus, we can safely infer that the dominant features that appear in the upwind and downwind zones in the 2D simulations will also appear in the 3D simulations. However, for low TSR, when α is in a post-stall region, the span-wise dissipation of the vortices significantly effects the forces on the airfoil and the 2D simulations will generally not closely follow their 3D counterparts.

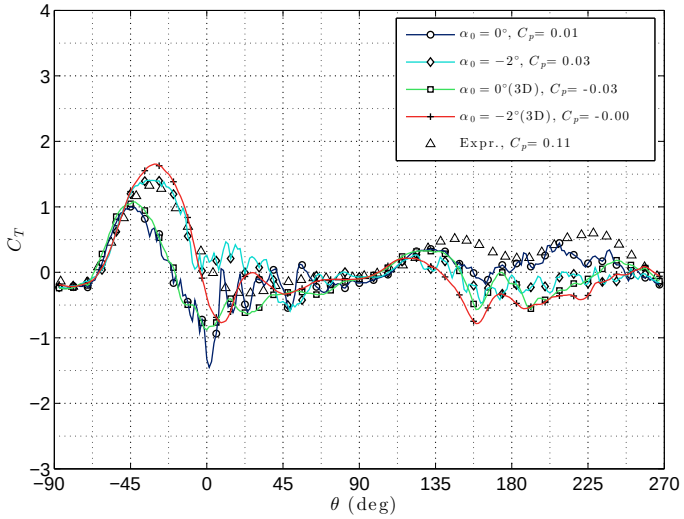

Figure 6. Tangential force of a VAWT blade as a function of azimuthal position for simulations in 2D and 3D $\alpha_0 = 0, -2°$ at $\lambda = 2.5$.

III.B. Parameterization Study: Pitch Angle Offset

In order to recreate the experiments performed in Ref. 8, parameterization studies were performed for the experimental parameters that were not reported or reported with a certain degree of uncertainty. The authors report that discrepancies in the experimental data, *"may be due to misalignment errors in the blade mounting... on the order of* 1° *in the blade angle of attack"*. In order to determine the pitch angle offset of the experimental turbine, relatively low-cost 2D ILES simulations were performed for $-5° \leq \alpha_0 \leq +5°$, in increments of 1° for $\lambda = 5.0$ and $T = 20°C$. As mentioned previously, the mounting point of the airfoil was taken to be a distance of $c/4$ from the leading edge. The blades were then rotated about this point by an angle of α_0. In these simulations, we found that any toe-in angle ($\alpha_0 > 0°$) of the airfoil decreased the efficiency of the turbine and led to a high variability in blade forces. Thus, in Fig. 7, we only show the tangential force coefficient of the VAWT as a function of the azimuthal angle for $\alpha_0 \geq 0°$ to improve readability. From Fig. 7, it is clear that $\alpha_0 = -3°$, denoted by '+' markers, has the largest maximum value

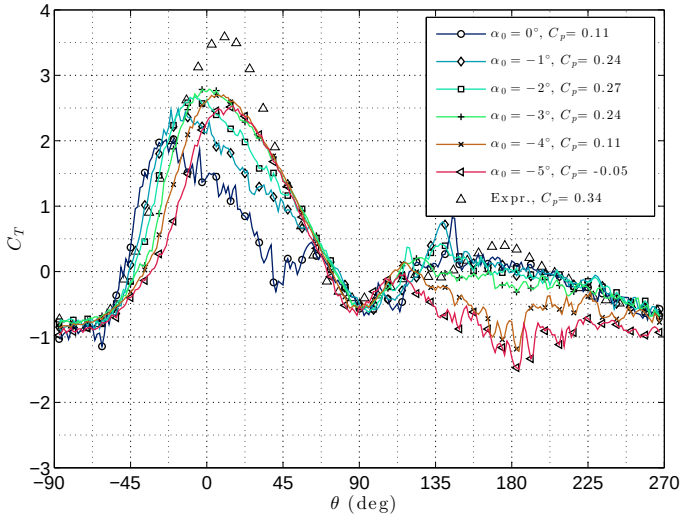

Figure 7. Tangential force of a VAWT blade as a function of azimuthal position for various α_0 at $T = 20°$, $\lambda = 5.0$

of any of the simulations. However, $\alpha_0 = -2°$, shown with open squares, has the largest power coefficient of the simulations ($C_p = 0.27$). This finding agrees very well with the data collected by Klimas and colleagues for the 5 m VAWT also built and tested by Sandia National Labs.[18] In these tests, which were performed

at various λ, the overall maximum power coefficient was achieved for $\alpha_0 = -2°$, ($C_p = 0.32$). Further, this pitch angle offset had the largest C_p for $3.5 \leq \lambda \leq 6.0$.

III.B.1. Parameterization Study: Temperature of Fluid

We were interested in the sensitivity of the forces on the turbine blades based on the temperature of the working fluid. The experiments were undertaken at a tow tank at Texas Tech University in Lubbock, Texas, where the temperature of the fluid could realistically vary by 5-10° depending on the building, insulation, season, etc. We varied the temperature on the order of $5°C$, to slightly change the Re of the flow and examined the numerical results. Though the simulations matched most closely for higher Re (corresponding to higher temperatures), we only thought it was reasonable to assume water temperature of at most $25°C$. The data for the kinematic viscosity of water as function of the temperature was found in Ref. 19. Figure 8 shows the tangential force coefficient as a function of azimuthal angle at $\lambda = 5.0$ and $\alpha_0 = -2°$ for various fluid temperatures $(20, 25, 30°C)$. Clearly, there is not a large change in the trend of the force as the

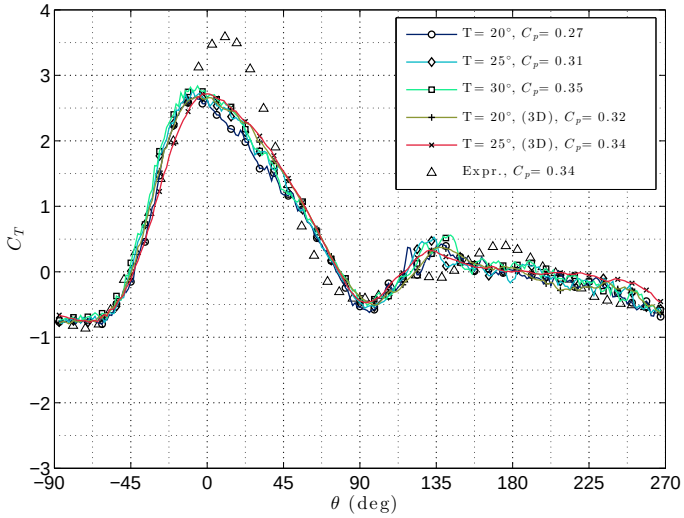

Figure 8. Tangential force of a VAWT blade as a function of azimuthal position for various T at $\alpha_0 = -2°$ and $\lambda = 5.0$

temperature changes by 5° or 10°. However, for these small temperature changes, we were not expecting such a large change in the turbine power coefficient, C_p. Figure 8 shows that a 5° increase in the temperature, which corresponds to a 10% increase in the Re number (due to the change in the kinematic viscosity of water), yields a 5% increase in power production. However, this increase is within the margin of variation of the torque variation from various passes of the turbine of blade. The 2D results, presented in Fig. 6 show a similar trend but to even a higher degree.

For a wind turbine exposed to environmental conditions the temperature of the fluid cannot be modified. However, this analysis shows that it is critical for researchers to report the temperature of the working fluid in controlled model tests (especially if they are performed in water) so that the conditions can be recreated in such numerical simulations.

III.C. Comparison with VAWT Analytical Models

Besides simulating the VAWT with ILES methods, two analytical codes were used to estimate the aerodynamic torque on the blades for comparison. A blade-element methodology called the Double Multiple Streamtube Method described in Ref. 20 was used along with a dynamic stall model of Berg.[21] This formulation uses a momentum method to model the streamwise wake deficit both in the 'upwind zone' and 'downwind zone' of the rotor (see Fig. 3 for depiction of zones) by iteratively solving for an induction factor. Once this factor is known in the upwind zone for all azimuthal angles, the force on the blades in the downwind zone can be determined. Also, a vortex method developed at Sandia National Laboratories called Code for Axial and Cross-flow TUrbine Simulation (CACTUS)[22] was used to simulate the aerodynamic torque. As of

2013, this numerical method was made available to public as an open-source software [a]. In this model, the data from the twentieth revolution of the turbine was used in order to allow the code to reach a steady-state solution. After corresponding with the authors of the code, the number of blade elements was increased to 10, which slightly improved the accuracy of the code. The sectional lift and drag coefficients for both of the codes came from the experimental data of Refs. 23 and 24. For these codes, the angle of attack was calculated at the mid-chord, as recommended in Ref. 8.

The experimental data of the tangential force coefficient shown as triangles in Figs. 9, 10 and 11 was taken as a blade swept over the first half of its fourth revolution (the only tabular data provided in Ref. 8). Due to the computational intensity of the ILES, the data from the ILES 2D and 3D simulations were taken from the forces on 'Blade 2' as it made its first pass from $-90° \leq \theta \leq 270°$ after starting from $\theta(t = 0) = -270°$. However, subsequent revolutions exhibited similar behavior, which was in agreement with the experimental data. The data from CACTUS was taken at 32 instances on the twentieth revolution of the simulation. The DMST only estimates the torque on the blades as an average for a single revolution (no unsteady effects) but the resolution can be increased by increasing the number of streamtubes.

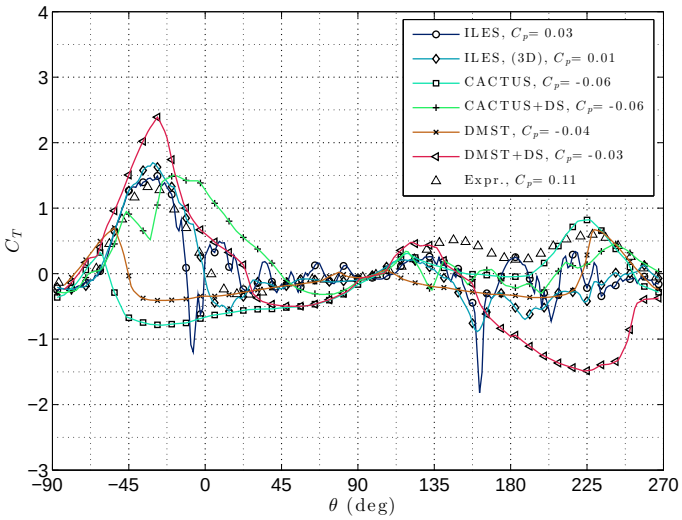

Figure 9. Tangential force of a VAWT blade as a function of azimuthal position λ=2.5

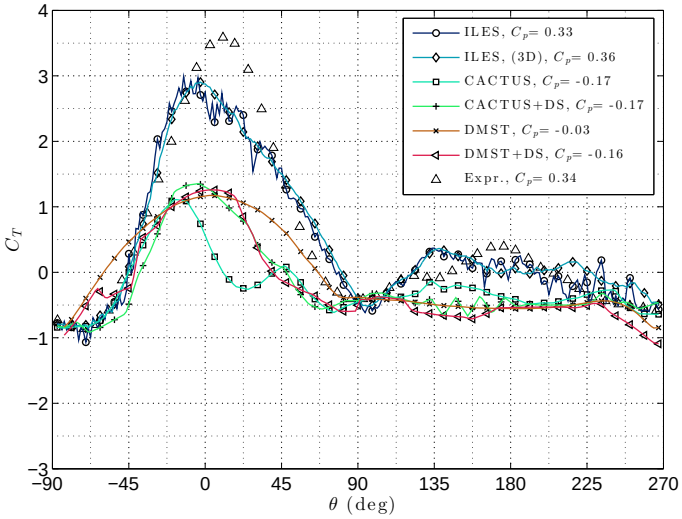

Figure 10. Tangential force of a VAWT blade on a straight-bladed turbine as a function of azimuthal position for λ=5.0

Figures 9, 10 and 11 show that the ILES simulation can approximate the experimental data very well at high TSR, especially in the downwind section. At λ=2.5, the CACTUS model utilizing the Leishman-Beddos

[a]At the time of publication, CACTUS is available at `http://energy.sandia.gov/?page_id=16734`

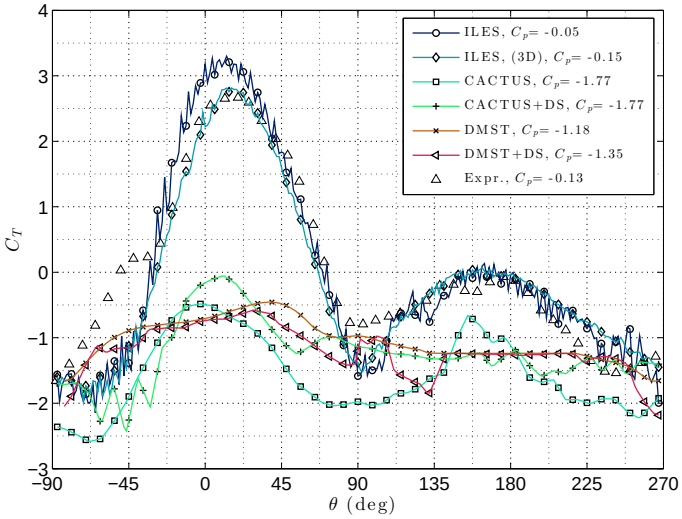

Figure 11. Tangential force of a VAWT blade as a function of azimuthal position for λ=7.5

dynamic stall model (described in Ref. 25) recreates the experimental data the best. However, at higher TSR the accuracy of the analytical models drops drastically resulting in highly inaccurate predictions for the power coefficients.

III.D. Flow Structure

Iso-surfaces of the q-criterion are frequently used to visualize the unsteady 3D flow structures in the fluid domain. The q-criterion physically represents areas where rotation dominates the strain of the flow. In the core of a columnar vortex, $q > 0$ since vorticity increases as the radial distance to the core decreases.[9] In Fig. 12, iso-surfaces of the q-criterion, where $q = 100$, are shown in 3D for various azimuthal angles of Blade 1 when $\lambda = 2.5$. As shown in the top row of Fig. 12, the azimuthal angle θ is 0° and columnar vortices are present in the downwind zone of the turbine. These vortices were shed in the wake of Blade 2 from its previous pass and then convected downstream due to the incident wind. The image to the right is a more detailed depiction of the iso-surfaces formed around Blade 1. At this instant in time, the angle of attack α is greater than 20°, excluding dynamic effects (see Fig. 1). Clearly, there are instantaneous vortical structures forming on the suction side of the airfoil. At $\theta = 60°$ these disturbances have formed into a more coherent structure, labeled 'Vortex A'. The location of Vortex A moves from the upwind zone into the downwind zone due to the influence of the incident wind throughout the time instances in Fig. 12. Interestingly, the vortices are convected too slowly to directly interfere with the flow field around Blade 1 when $120° \leq \theta \leq 180°$.

Interestingly, for a higher tip-speed ratio, the vortical structures in the wake of the airfoil still exist, albeit much less coherently and reduced in size. In Fig. 13, for λ=5.0, iso-surfaces of the q-criterion are plotted, colored by the velocity magnitude. In these plots the iso-surfaces are for q=10, (instead of 100) since the vorticity in the fluid surrounding the blades is significantly less. The azimuthal angles shown $0° - 90°$ were chosen to correspond to the time when the airfoil reaches a maximum angle of attack and when the vortices are dissipated by the surrounding fluid. While the vortical structures formed by the airfoils at λ=2.5 (e.g., 'Vortex A') are convected throughout the entire domain, the vortices shed at λ=5.0 (e.g., 'Vortex B') dissipate within a quarter-period. This finding corresponds with the results of a PIV study performed on a model vertical-axis wind turbine by Ferreira et al, documented in Ref. 26 (for a NACA0015 airfoil at $Re_\infty = 5 \cdot 10^5$). The size and strength of the regions of shed vorticity in the wakes of the blades decreased as λ increased. The PIV data showed that magnitude of the counter-clockwise vorticity decreased by an order of magnitude for only a two-fold increase of λ. Interestingly, for $\lambda \geq 4.0$ the authors reported no vortex detatchment from the airfoil. However, the strength and lifespan of 'Vortex B' are so small that the vortex may not be able to measured by modern PIV techniques. The strength of the vortices shed by an airfoil at high angle of incidence corresponds to the structure of the separated shear layer. At higher angles of attack (lower tip-speed ratios) the inflection point of the velocity profile is higher above the suction surface of the airfoil. Perhaps this feature has an effect on the size and strength of the vortices that are formed.

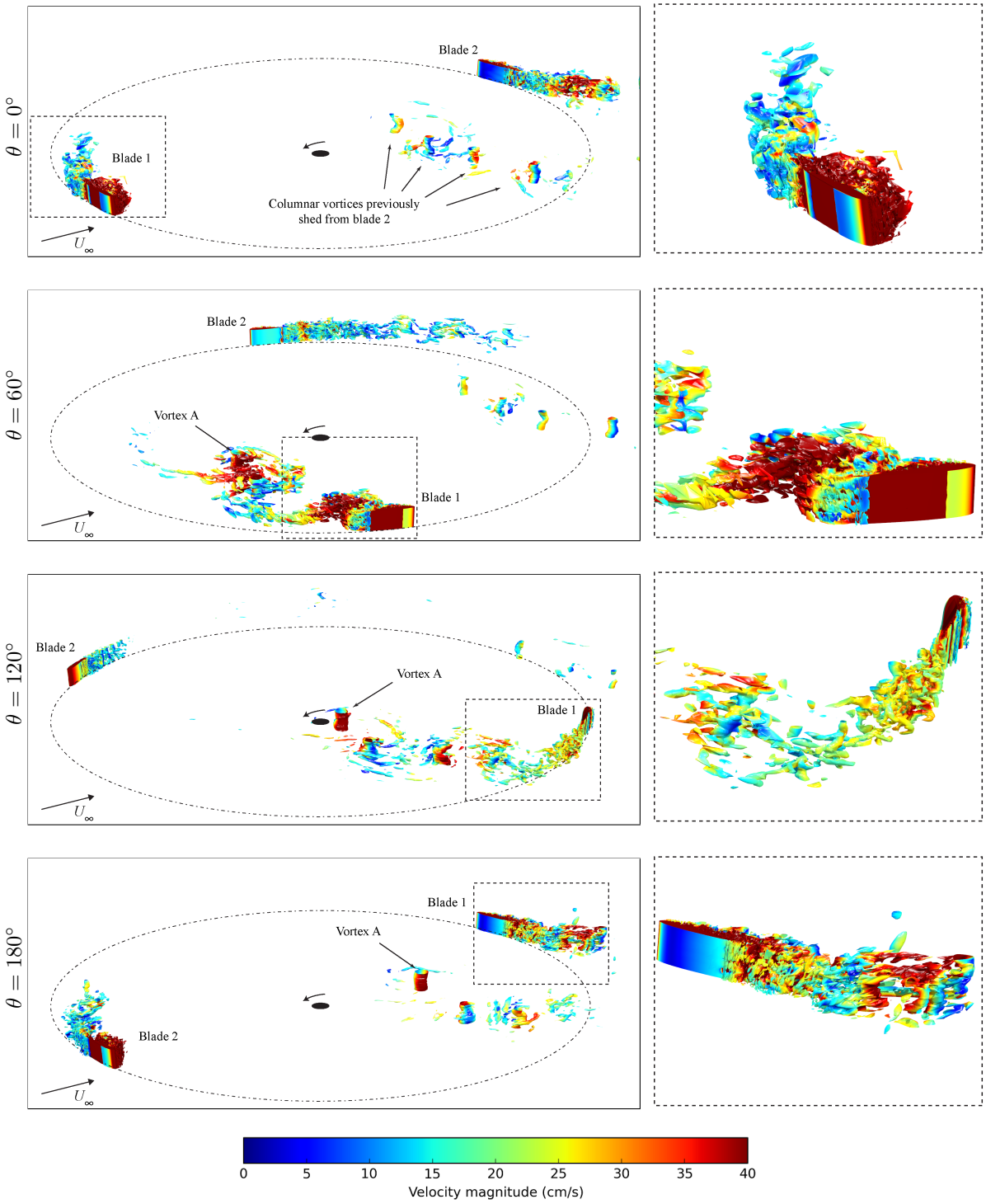

Figure 12. Iso-surfaces of the q-criterion for $q = 100$ at various azimuthal angles for a half-rotation of Blade 1 at $\lambda = 2.5$. Images on right are magnified views of Blade 1. The time evolution of 'Vortex A' is discussed in the text. The isosurfaces are colored according to the magnitude of the velocity, as indicated by the colorbar at the bottom of the figure.

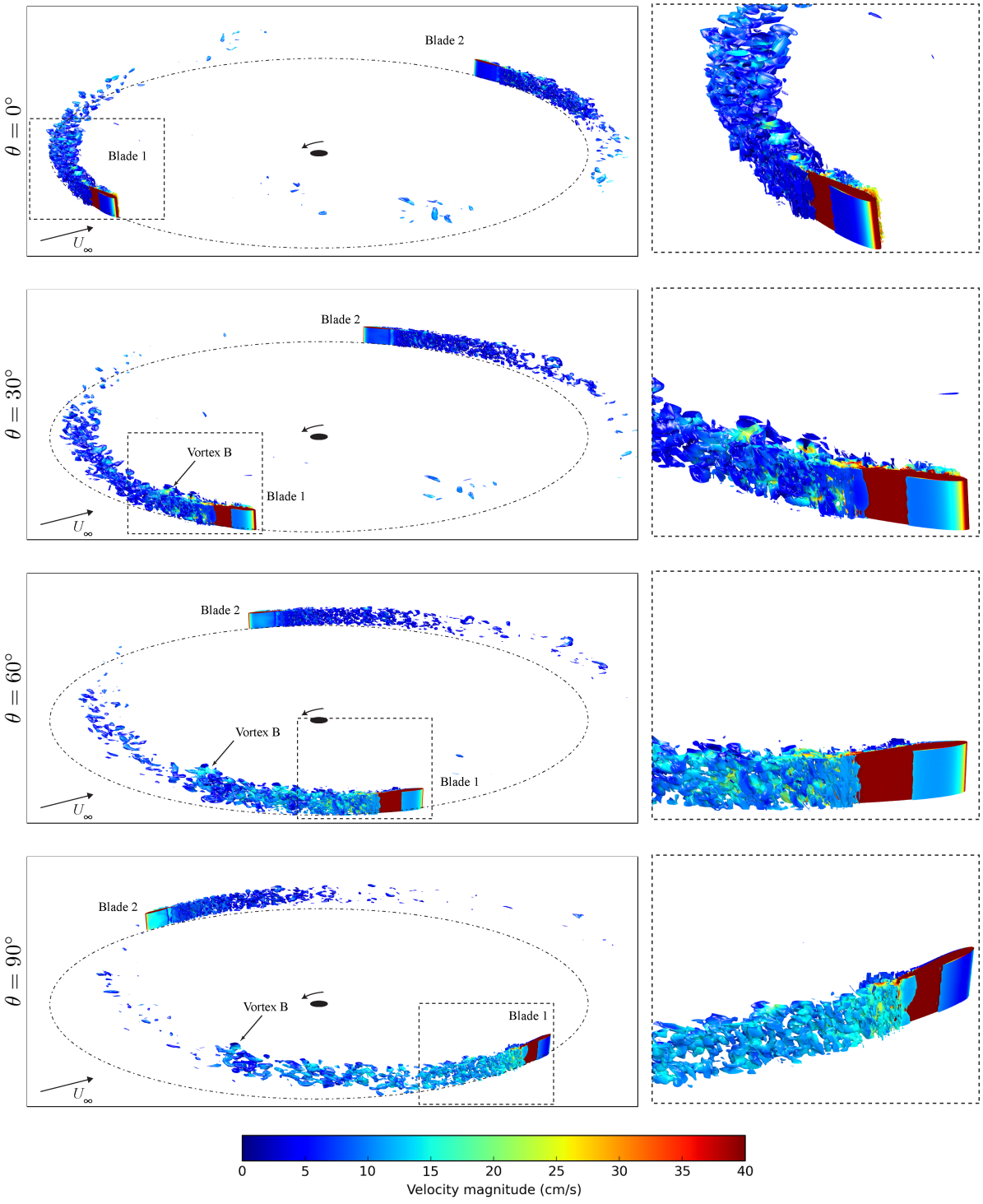

Figure 13. Iso-surfaces of the q-criterion for $q = 10$ at various azimuthal angles for a quarter-rotation of Blade 1 at $\lambda = 5.0$. Images on right are magnified views of Blade 1. The isosurfaces are colored according to the magnitude of the velocity, as indicated by the colorbar at the bottom of the figure (same scale as in Fig. 13).

III.E. Frequency Content

For one case, $\lambda = 5.0$, $T = 25°$, $\alpha_0 = -2°$, we ran an extra long simulation, far past the time where the results had reached a relatively periodic solution. Figure 14 shows the power spectral density of the tangential force coefficient as a function of the Strouhal number for the last 6 revolutions of the turbine. The dominant frequencies that were experienced by the turbine blade, multiplied by the period for one revolution of the turbine, are also shown. As expected for a time series with a sinusoidal peak in the first third of the period

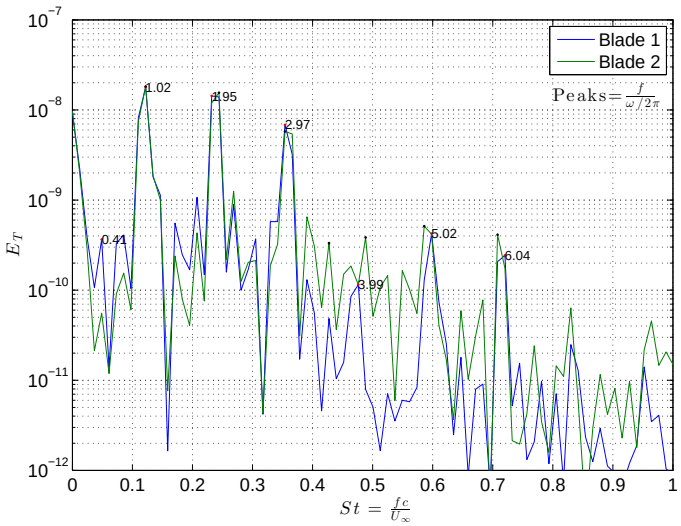

Figure 14. Power spectral density of tangential force coefficient of 3D turbine for 6 rotations at λ=5.0.

and then near zero for the rest of the period (see Fig. 10), the dominant frequencies are the first few integer multiples of the turbine revolution period. However, the PSD of these peaks should decay exponentially. Interestingly the peaks around 5 and 6 times the revolution period are quite large. Furthermore, the St range of 0.6-0.7 is similar to the dominant frequency of the forces on a static NACA0012 airfoil at $\alpha = 12°$ found using DNS[27] ($Re = 5.0 \cdot 10^4$, St=0.612). We hope to explore whether these frequencies are stemming from vortex shedding events or are just figments of the spectral analysis of this particular time-series.

IV. Conclusions

ILES simulations of a rotating VAWT at a range of TSRs were performed. The results from the VAWT simulations showed that the 2D simulations were accurate at high TSR ($\lambda \geq 5.0$). At these TSRs, the maximum angle of attack can exceed 12°, which corresponds to the static post-stall regime for a NACA0012 airfoil. Yet, these 2D simulations, which failed to accurately predict the forces for a static airfoil at these angles of attack, can simulate the forces for the entire turbine fairly accurately. However, these 2D results had high frequency components that were not present in the results from the 3D simulations. From this, we infer that the span-wise length of the airfoil has an averaging effect on the tangential force on the blade. We also confirmed the results of previous researchers that a small toe-out angle can increase the efficiency of the VAWT by nearly 10%. Further, small changes in the viscosity (or temperature) of the fluid can have an influence on the forces on the turbine blades. We believe that many of the structural problems VAWTs have had are due to the relatively unknown frequency content of the aerodynamic torque applied to the structure. In the future we hope to be able to describe the mechanism of why certain frequencies exist in the power spectral density. We also hope to clarify whether these frequencies would exist with larger spans of the simulated blade. Further, we hope to push the Re number of the simulations higher through the use of Detached Eddy simulation (DES) techniques.

Acknowledgements

The first author was supported by the Department of Defense (DoD) through the National Defense Science & Engineering Graduate Fellowship (NDSEG) Program as well as the National Science Foundation

(NSF) through the Graduate Research Fellowship Program. The first author would also like to thank his PhD adviser, Prof. R.W Yeung, as well as Matthew Barone of Sandia National Laboratories. This research used resources of the National Energy Research Scientific Computing Center, a DOE Office of Science User Facility supported by the Office of Science of the U.S. Department of Energy under Contract No. KJ04-01-00-0.

References

[1]Roddier, D., Cermelli, C., Aubault, A., and Weinstein, A., "WindFloat: A floating foundation for offshore wind turbines," *Journal of Renewable and Sustainable Energy*, Vol. 2, No. 3, June 2010, pp. 033104.

[2]Sutherland, H. J., Berg, D. E., and Ashwill, T. D., "A retrospective of VAWT technology," *Sandia National Laboratories*, 2012.

[3]Srensen, N. N. and Michelsen, J. A., "Drag Prediction for Blades at High Angle of Attack Using CFD," *Journal of Solar Energy Engineering*, Vol. 126, No. 4, Nov. 2004, pp. 1011–1016.

[4]Gao, H., Hu, H., and Wang, Z. J., "Computational study of unsteady flows around dragonfly and smooth airfoils at low Reynolds numbers," *46th AIAA Aerospace Sciences Meeting and Exhibit*, 2008, pp. 7–10.

[5]Li, C., Zhu, S., Xu, Y.-l., and Xiao, Y., "2.5 D large eddy simulation of vertical axis wind turbine in consideration of high angle of attack flow," *Renewable energy*, Vol. 51, 2013, pp. 317–330.

[6]Smagorinsky, J., "General Circulation Experiments with the Primitive Equations," *Monthly Weather Review*, Vol. 91, 1963, pp. 99.

[7]Mueller, T. J. and DeLaurier, J. D., "Aerodynamics of Small Vehicles," *Annual Review of Fluid Mechanics*, Vol. 35, No. 1, 2003, pp. 89–111.

[8]Strickland, J. H., Smith, T., and Sun, K., "Vortex Model of the Darrieus Turbine: An Analytical and Experimental Study. Final Report," Tech. Rep. SAND-81-7017, Sandia National Labs., Albuquerque, NM (USA); Oregon State Univ., Corvallis (USA). Dept. of Mechanical Engineering, June 1981.

[9]Uranga, A., Persson, P.-O., Drela, M., and Peraire, J., "Implicit Large Eddy Simulation of transition to turbulence at low Reynolds numbers using a Discontinuous Galerkin method," *International Journal for Numerical Methods in Engineering*, Vol. 87, No. 1-5, July 2011, pp. 232–261.

[10]Froehle, B. M., *High-Order Discontinuous Galerkin Fluid-Structure Interaction Methods*, Ph.D. thesis, University of California, Berkeley, 2013.

[11]Wang, Z., Fidkowski, K., Abgrall, R., Bassi, F., Caraeni, D., Cary, A., Deconinck, H., Hartmann, R., Hillewaert, K., Huynh, H., Kroll, N., May, G., Persson, P.-O., van Leer, B., and Visbal, M., "High-order CFD methods: current status and perspective," *Internat. J. Numer. Methods Fluids.*, Vol. 72, No. 8, 2013, pp. 811–845.

[12]Persson, P.-O., Bonet, J., and Peraire, J., "Discontinuous Galerkin solution of the Navier-Stokes equations on deformable domains," *Comput. Methods Appl. Mech. Engrg.*, Vol. 198, No. 17–20, 2009, pp. 1585–1595.

[13]Peraire, J. and Persson, P.-O., "High-order discontinuous Galerkin methods for CFD," *Adaptive high-order methods in computational fluid dynamics*, Vol. 2 of *Adv. Comput. Fluid Dyn.*, World Sci. Publ., Hackensack, NJ, 2011, pp. 119–152.

[14]Peraire, J. and Persson, P.-O., "The compact discontinuous Galerkin (CDG) method for elliptic problems," *SIAM J. Sci. Comput.*, Vol. 30, No. 4, 2008, pp. 1806–1824.

[15]Strickland, J. H., Webster, B. T., and Nguyen, T., "Vortex Model of the Darrieus Turbine: An Analytical and Experimental Study." Tech. Rep. SAND-79-7058, Sandia National Labs., Albuquerque, NM (USA); Oregon State Univ., Corvallis (USA). Dept. of Mechanical Engineering, June 1979.

[16]Persson, P.-O. and Strang, G., "A simple mesh generator in Matlab," *SIAM Rev.*, Vol. 46, No. 2, 2004, pp. 329–345.

[17]Persson, P.-O. and Peraire, J., "Curved mesh generation and mesh refinement using Lagrangian solid mechanics," *47th AIAA Aerospace Sciences Meeting and Exhibit, Orlando, Florida*, Jan. 2009, AIAA-2009-949.

[18]Klimas, P. and Worstell, M. H., "Effects of blade preset pitch/offset on curved-blade darreius vertical-axis wind turbine performance." Tech. Rep. SAND-81-1762, Sandia National Labs., Albuquerque, NM ,USA, 1981.

[19]Okiishi, M. Y., Munson, B., and Young, D., "Fundamentals of Fluid Mechanics," *John Wiley & Sons, Inc*, 2006.

[20]Paraschivoiu, I., *Wind turbine design: with emphasis on Darrieus concept*, Presses inter Polytechnique, 2002.

[21]Berg, D. E., "Improved double-multiple streamtube model for the Darrieus-type vertical axis wind turbine," *Presented at the Am. Solar Energy Soc. Meeting, Minneapolis, 1 Jun. 1983*, Vol. 1, 1983.

[22]Barone, M. F. and Murray, J., "The development of CACTUS: a wind and marine turbine performance simulation code." Tech. rep., Sandia National Laboratories, 2010.

[23]Alam, M. M., Zhou, Y., Yang, H. X., Guo, H., and Mi, J., "The ultra-low Reynolds number airfoil wake," *Experiments in Fluids*, Vol. 48, No. 1, Jan. 2010, pp. 81–103.

[24]Ohtake, T., Nakae, Y., and Motohashi, T., "Nonlinearity of the aerodynamic characteristics of NACA0012 aerofoil at low Reynolds numbers," *Japan Society of Aeronautical Space Sciences*, Vol. 55, 2007, pp. 439–445.

[25]Leishman, J. G. and Beddoes, T. S., "A generalised model for airfoil unsteady aerodynamic behaviour and dynamic stall using the indicial method," *Proceedings of the 42nd Annual Forum of the American Helicopter Society, Washington DC*, 1986.

[26]Ferreira, C. S., Kuik, G. v., Bussel, G. v., and Scarano, F., "Visualization by PIV of dynamic stall on a vertical axis wind turbine," *Experiments in Fluids*, Vol. 46, No. 1, Jan. 2009, pp. 97–108.

[27]Rodrguez, I., Lehmkuhl, O., Borrell, R., and Oliva, A., "Direct numerical simulation of a NACA0012 in full stall," *International Journal of Heat and Fluid Flow*, Vol. 43, Oct. 2013, pp. 194–203.